Molecular Crystals and Liquid Crystals
Publication details, including instructions for authors and subscription information:
http://www.tandfonline.com/loi/gmcl20

# All-Optical Switching and Filtering Based on Liquid Crystals and Photosensitive Composite Organic Materials

Rita Asquini [a] & Antonio d'Alessandro [a]
[a] Department of Information Engineering, Electronics and Telecommunications , Sapienza University of Rome , Rome , Italy
Published online: 02 Apr 2013.

To cite this article: Rita Asquini & Antonio d'Alessandro (2013) All-Optical Switching and Filtering Based on Liquid Crystals and Photosensitive Composite Organic Materials, Molecular Crystals and Liquid Crystals, 572:1, 13-23, DOI: 10.1080/15421406.2012.763205

To link to this article: http://dx.doi.org/10.1080/15421406.2012.763205

*Mol. Cryst. Liq. Cryst.*, Vol. 572: pp. 13–23, 2013

ISSN: 1542-1406 print/1563-5287 online
DOI: 10.1080/15421406.2012.763205

Taylor & Francis
Taylor & Francis Group

# All-Optical Switching and Filtering Based on Liquid Crystals and Photosensitive Composite Organic Materials

RITA ASQUINI* AND ANTONIO d'ALESSANDRO

Department of Information Engineering, Electronics and Telecommunications, Sapienza University of Rome, Rome, Italy



*We present our recent experimental results on guided wave devices that can be switched and tuned by optical driving signals. Two different waveguide structures recently implemented are reported. The first one uses liquid crystals (LCs) as a core in a $SiO_2$/Si V-groove and optical signals whose power is in the order of few milliwatts to control propagation. The second structure is an all-optical tunable filter that includes photosensitive composite materials. The latter combines the simple and low-cost ion exchange waveguide technology with a composite LC methyl red azo-dye photosensitive compound to obtain full optical tunability.*

**Keywords** All-optical devices; liquid crystals; nonlinear optics; organic materials

## 1. Introduction

An increasing interest is being paid to all-optical devices to fulfil the requirements of next-generation optical networks [1–4]. In fact, optical technologies allow much larger bandwidths for data transport and switching as compared with electronic ones. High-speed interconnections with Tbit/s rates without electronic bottleneck seem to be just around the corner. Recently, an all-optical fast Fourier transform channel with a single light source transmitting 26 Tbit/s has been demonstrated [5]. Furthermore, components allowing all-optical control and a built-in tunability can be successfully used in optofluidic systems for biosensing [6–8] and biomedical applications [9]. Liquid crystals (LC) [10–12] and doped LC novel materials [13,14] with their large electro-optic effect and nonlinear optical properties allow the production of low-cost optoelectronic devices for various applications in photonics [15–18] and optofluidics [19–21].

Guided-wave devices using an LC core can operate in both linear and nonlinear optical regimes. As linear waveguides, they can behave as variable optical attenuators as well as optical switches by exploiting the electrooptic effect in nematic LC (NLC) [22–25]. An applied voltage lower than 5 V was required to drive an electro-optic switch (EOS) with an on-off contrast of more than 40 dB [25]. Bragg reflectors based on LC waveguides (LCWs) that can be electro-optically tuned by an applied voltage have been reported [26–31]. A voltage-tunable distributed feedback grating in an LCW with coplanar electrodes has been

*Address correspondence to Rita Asquini, Department of Information Engineering, Electronics and Telecommunications, Sapienza University of Rome, Rome, Italy. Tel.: +0039 0644585834; Fax: +0039 0644585918. E-mail: rita.asquini@uniroma1.it

also designed [32]. The device allows transverse light confinement and periodic index modulation, with high reflectivity in a wide tuning range exceeding 100 nm for applied voltages between 2.5 and 10.2 V.

Several devices exploiting nonlinear effects in an LC core have been proposed, as well.

All-optical infrared light modulators in channel waveguides infiltrated with an NLC have been recently demonstrated in a silica-on-silicon V-groove [33,34] and proposed in an SU8 rectangular hollow one [35]. All-optical tunable filters can also be obtained by using a mixture of azo-dye-doped LC [36,37]. Nonlinear induced self-guided beams in NLCs and dye-doped NLCs have been experimentally investigated too [38–41], and all-optical switching with spatial solitons has been demonstrated [42,43].

In this paper, we present our recent experimental results on two different channel optical waveguide devices, which can be optically switched and tuned. They are based on LCs and methyl red (MR) azo-dye compounds. The first device is produced infiltrating NLC E7 in a recessed triangular silicon groove. The second one in an all-optical filter and consists of a POLICRYPS (POlymer LIquid CRYstal Polymer Stripes) grating structure of alternating stripes of polymer NOA61 and E7 NLC doped with MR overlaying a double ion-exchange glass channel optical waveguide. Experimental characterization and nonlinear propagation properties of both structures are reported and discussed.



## 2. Optically Controlled LCW on Silicon

An exploded view of the all-optical LCW device is reported in Fig. 1(a). The device consists of a channel waveguide made of silica thermally grown on silicon ($SiO_2$/Si) shaping a V-groove filled with NLC E7. The top cover is a borosilicate glass (Schott D263) coated with an indium tin oxide (ITO) layer, which can be used to contact the device. A Nylon 6 layer is rubbed on the ITO layer in order to promote an alignment of the NLC molecules along the propagation direction. The V-groove triangular profile is obtained through the anisotropic preferential etching of the (100) oriented silicon substrate with a 54.7° base angle. The upper width of the triangular section can range from 10 to 15 $\mu$m. The silicon dioxide grown by thermal oxidation has a thickness of 2 $\mu$m along the (111) plane and 1.5 $\mu$m along the (100) plane. The $SiO_2$ layer has a lower refractive index compared with Si; therefore, $SiO_2$ can be used as optical buffer. Silicon wafer is 380 $\mu$m thick and has a

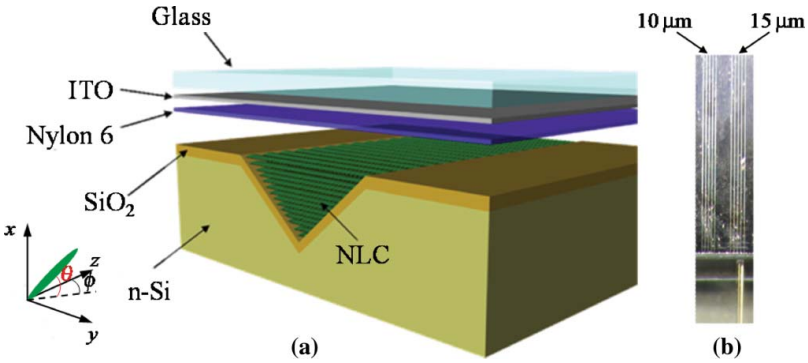


**Figure 1.** Structure of an all-optical liquid crystal waveguide device made infiltrating E7 nematic liquid crystal in a triangular silicon groove (a) and produced prototype with sets of 10- and 15-$\mu$m-width NLC straight waveguides (b).

resistivity of about 10 Ω·cm. The ITO thickness is 100 nm and has a sheet resistance of 80 Ω/square. UV adhesive NOA61 by Norland is used to seal the V-groove channel. Fig. 1(b) is a photograph under a polarized microscope of $SiO_2$/Si waveguides sets made in a single n-type silicon substrate. The lower side of Fig. 1(b) shows the fiber used to launch the optical signal into an LCW. The device structure and realization steps are detailed in previous papers [25,44].

### *2.1. LCW on Silicon: Working Principle and Model*

The working principle of the LCW on silicon is based on the confinement of the propagating light obtained through the modulation of the LC's effective refractive index. Molecular tilt reorientation in the LC can be achieved by applying an electric field, through the application of a voltage between n-Si and ITO electrodes (linear propagation) and/or by the propagating optical beam itself. Light propagation occurs when the NLC's refractive index, dependent on molecular distribution, is higher than the glass–$SiO_2$ surrounding materials. A voltage bias of about 2 V is applied to induce a molecular tilt over the Fredericks threshold. As a consequence, all-optical control is obtained with a relatively high power of the propagating light beam in the order of tens of milliwatts, exploiting the optical Freedericks transition.

Modeling of the induced reorientation effects on light propagation in the LCW has been carried out in the near-infrared wavelengths [34,45]. The LC director spatial distribution is calculated through the minimization of the free energy $F = F_e + F_d + F_{opt}$ [10] being:

$$F_e = \frac{1}{2}\iiint_v \{k_{11}(\nabla \cdot \vec{n})^2 + k_{22}[\vec{n} \cdot (\nabla \times \vec{n})]^2 + k_{33}[\vec{n} \times (\nabla \times \vec{n})]^2\} dv, \tag{1}$$

$$F_d = -\frac{1}{2}\iiint_v \varepsilon_0[\Delta\varepsilon_d(\vec{n} \cdot \vec{E})^2 + \varepsilon_{\perp,d}\vec{E} \cdot \vec{E}] dv, \tag{2}$$

$$F_{opt} = -\frac{1}{2}\iiint_v \varepsilon_0[\Delta\varepsilon_{opt}(\vec{n} \cdot \vec{E}_{opt})^2 + \varepsilon_{\perp,opt}\vec{E}_{opt} \cdot \vec{E}_{opt}]\, dv, \tag{3}$$

where $F_e$ is the elastic energy (with $k_{11}$, $k_{22}$, and $k_{33}$ being elastic constants of the NLC for splay, twist, and bend deformation, respectively), $F_d$ is the dielectric energy, and $F_{opt}$ is the optical energy, with the integrals computed over the NLC volume $v$, and $\varepsilon_d$ being the dielectric anisotropy, $\varepsilon_{\perp,d}$ the dielectric constant perpendicular to the NLC director at low frequencies, and $\varepsilon_{opt}$ and $\varepsilon_{\perp,opt}$ the values at optical frequencies, respectively. The electric field $\vec{E}$ results from the application of a voltage to the electrodes and $\vec{E}_{opt}$ is the electric field due to the propagating light beam with fairly high intensity.

A finite-element method was used to solve the partial derivative Euler–Lagrange equation for the minimization of the free energy. The obtained director spatial distribution was used to study the propagation of an optical beam in the LCW with a beam propagator. The refractive indexes used in the modeling at the wavelength of 1550 nm are: $n_{||} = 1.689$ and $n_{\perp} = 1.502$, referred to LC E7 (for light polarization parallel and perpendicular to the director, respectively), $n_{SiO2} = 1.444$ for silica, $n_{Si} = 3.478$ for silicon, $n_{D263} = 1.516$ for glass corning D263, and $n_{NOA61} = 1.542$ for NOA61 UV adhesive. The complete theoretical study can be found in [45].

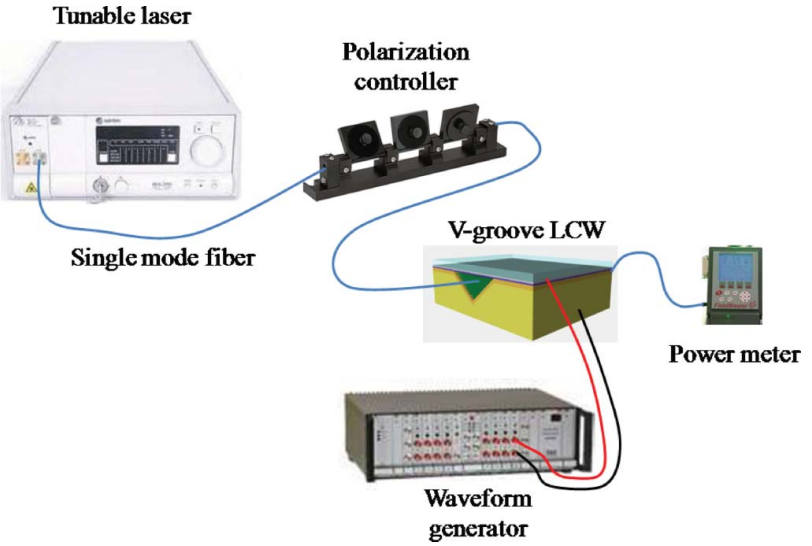


**Figure 2.** Experimental setup used for nonlinear optical characterization of the V-groove LCW.

### *2.2. LCW on Silicon: Nonlinear Optical Characterization*

The device characterization in the optical nonlinear regime has been carried out by using the setup reported in Fig. 2. An optical signal sourced from a tunable laser in the range 1510–1590 nm is driven through a single-mode fiber butt-coupled to the V-groove LCW. A polarization controller is inserted between the laser source and the device in order to select the desired polarization state, minimizing the optical power loss. Output optical power is collected through an optical fiber butt-coupled to the output V-groove and measured with an optical power meter. A waveform generator is used to apply a bias voltage to the sample in order to provide a LC director pretilt over the Fredericks threshold. In particular, a square waveform of frequency 1 kHz with variable amplitude can be effectively used as bias voltage. Further director reorientation is due to all-optical modulation obtained for increasing input power of the laser beam from 10 mW till about 25 mW.

Figure 3 shows the experimentally measured output optical power versus the input one (a), compared with the computed values (b), at different bias voltages (6 V and 6.7 V for the measured values, 2.16 V and 2.17 V for the numerical results). A nonlinear behavior is observed in Fig. 3(a) for the plot corresponding to 6 V when the input power increases over 12 mW. The nonlinear trend has a greater emphasis in the 6.7 V plot, where input power increases even above 10 mW. The plots obtained for bias voltages 2.16 V and 2.17 V depict well the measurements obtained for 6 V and 6.7 V, respectively. The difference between bias voltages in simulations and experimental results depends on the presence of defects on the groove surface perturbing the LC molecular orientation (not included in the model). Moreover, a further difference can be attributed to the voltage drop at the electrodes, which smoothes out the square waveform, causing a reduction of the RMS voltage. At voltages higher than 8 V, maximum transmission is reached and the behavior becomes linear again.

### *2.3. LCW on Silicon Used as Nonlinear Optical Switch*

Once the V-groove LCW was characterized, proving the possibility to control the output optical signal through self-modulation of the input optical signal, the device has been tested

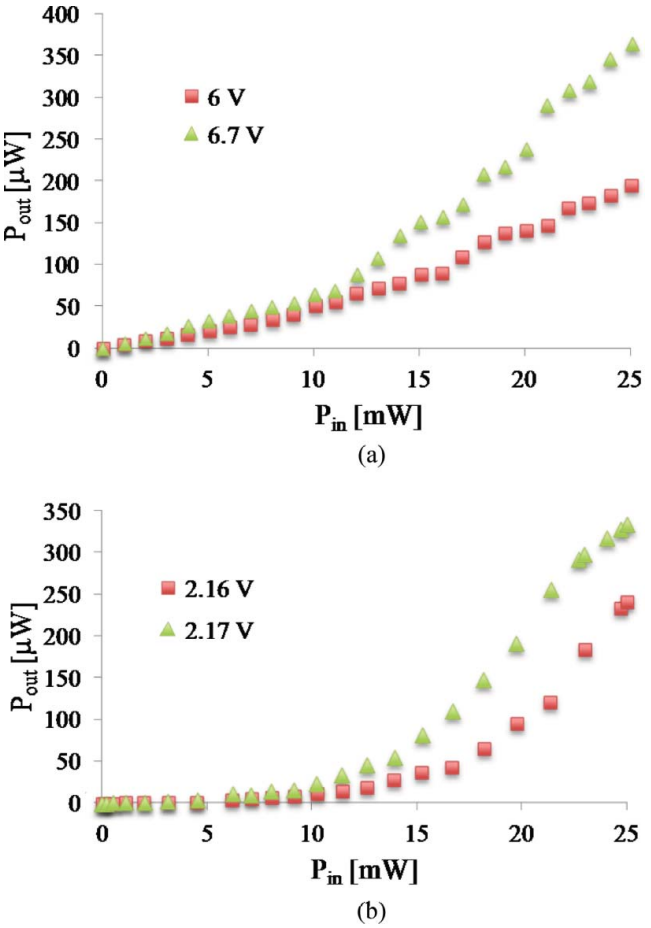


**Figure 3.** Experimental (a) and numerical (b) results of the LCW nonlinear behavior.

as an all-optical switch by means of the setup presented in Fig. 4. Two optical signals are multiplexed and sent to the LCW. The optical signal wavelength indicated as $\lambda_s = 1510$ nm is generated by the probe diode laser with 2 mW power. The optical control signal wavelength indicated as $\lambda_p = 1560$ nm is provided by a pump diode laser with 20 mW power. Both signals are transverse magnetic (TM) polarized through a $\lambda/4-\lambda/2-\lambda/4$ wave plate before being multiplexed. The sample is biased with a square wave voltage of 6.7 V amplitude at 1 kHz frequency supplied by a waveform generator. The output optical signal is measured by an OSA. An EOS is used to switch on and off the pump signal.

Figure 5 shows the output signal detected by the OSA, confirming the possible use of the LCW as an all-optical switch. When the pump signal is off ($\lambda_p$ off) and just the probe laser signal is sent to the LCW, the output peak at 1510 nm is about $-56$ dBm (Fig. 5(a)). After switching on the pump signal ($\lambda_p$ on) to just 20 mW, the output probe signal is raised by over 11 dB, at about $-45$ dBm (Fig. 5(b)).

The preliminary experiment presented proves that the simple LCW V-groove here reported can be used as all-optical shutter, with a contrast of about 13:1 with an optical driving signal of just 20 mW.

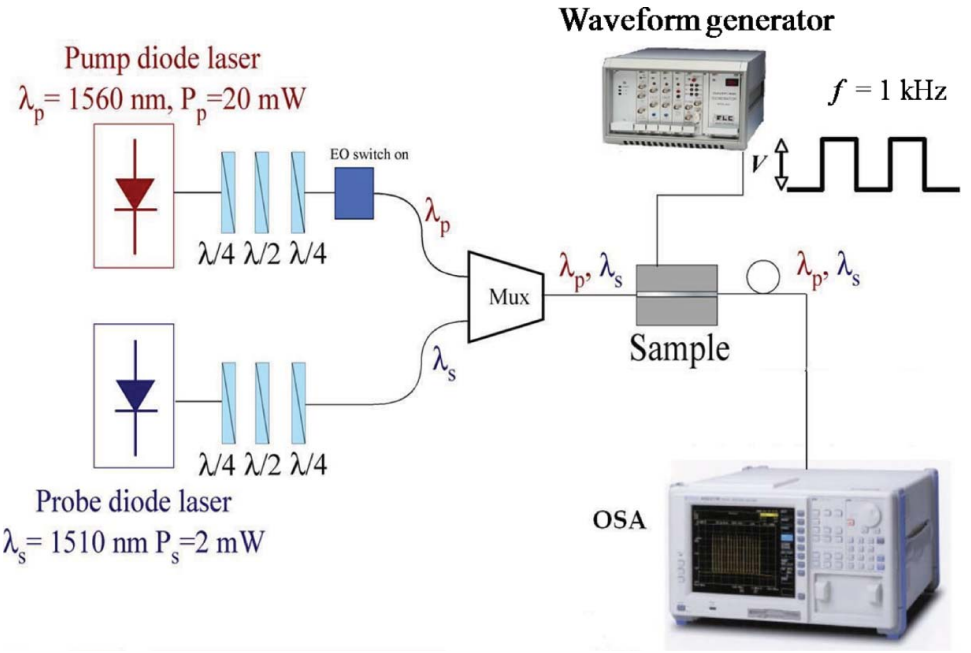


**Figure 4.** Experimental setup used to demonstrate all-optical switching of the LCW.

## 3. All-Optical Tunable Filter with Photosensitive Composite Materials

A polarization-independent all-optical and tunable Bragg filter made with a composite POLICRYPS structure using a photosensitive azo-dye-doped NLC has been recently demonstrated [37]. The device is described here briefly and the experimental results obtained with a real sample device are reported.

Figure 6(a) is a sketch of the all-optical filter, and Fig. 6(b) is a photograph of a realized prototype during its characterization. The device consists of a composite grating structure made of alternated stripes of polymer NOA 61 (by Norland) and azo-dye MR-doped NLC E7 sandwiched between two BK7 glass, with a channel waveguide ion-diffused in the glass substrate (the upper glass is not depicted in Fig. 6(a) to simplify the sketch). The diffused channel waveguide is obtained with a $K^+-Na^+$/ $Ag^+-Na^+$ double ion-exchange process in BK7 glass. Afterward, the top glass substrate is placed with a 1-$\mu$m gap between the two glasses obtained by means of ball spacers mixed to UV glue NOA 61. In order to obtain the composite grating, a POLICRYPS structure is first realized [46], then the NLC inside the POLICRYPS is removed and replaced with NLC E7 doped with MR (MR:E7). A quantity of 2% in weight of MR in NLC E7 is chosen in order to minimize the pump power required for optical switching [47].

### *3.1. All-Optical Tunable Filter Working Principle*

The device behaves as a Bragg filter because a transverse electric (TE)-like optical beam launched in the channel waveguide experiences the overlaying phase grating. The back-reflected wavelength $\lambda_B$ is given by the Bragg law:

$$\lambda_B = \frac{2\Lambda n_{\text{eff}}}{m}, \tag{4}$$

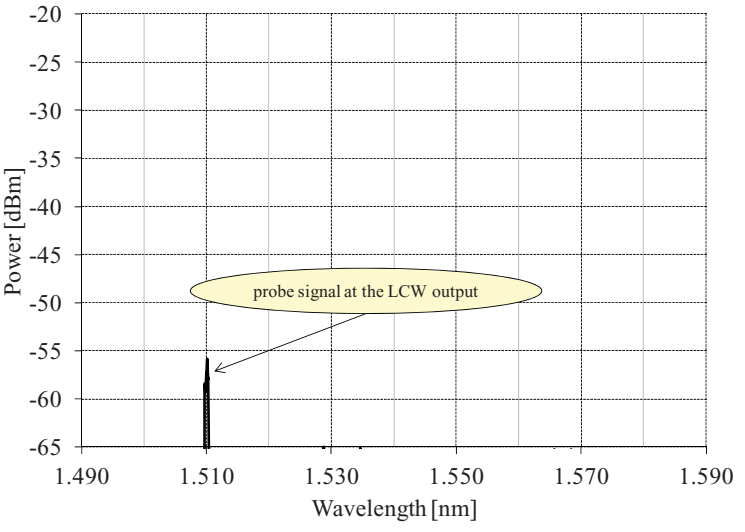


(a)

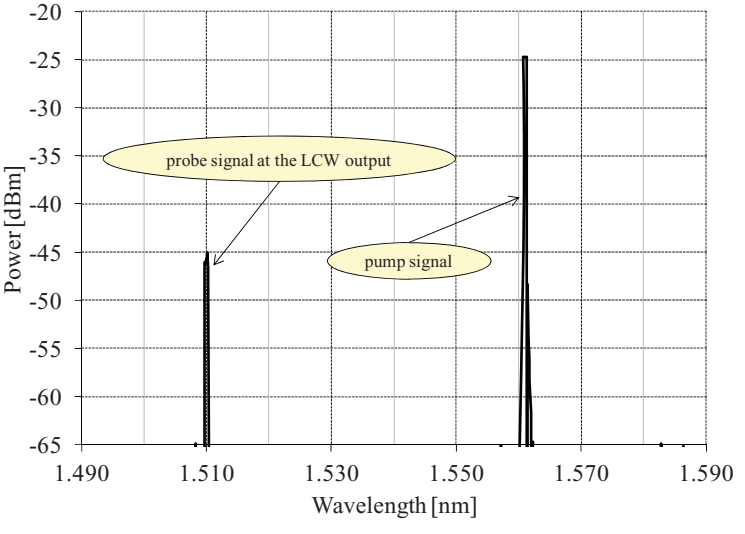


(b)

**Figure 5.** Output probe laser signals at 1510 nm detected by the optical spectrum analyzer during all-optical switching with the V-groove LCW (a) without and (b) with a light pump signal at 1560 nm.

being $\Lambda$ the grating period, $n_{\text{eff}}$ the effective refractive index of the guided mode, and $m$ the grating diffraction order.

At thermal equilibrium, the MR is in its elongated *trans* form, and long axis of both LC molecules and *trans*-MR are aligned perpendicularly to the polymer slices (along $z$-axes in Fig. 6(a)). In this case, the phase grating is due to the mismatch between the *trans*-MR:E7 ordinary refractive index being about 1.5 at 1550 nm (approximately equal to the E7 LC ordinary refractive $n_{\perp} = 1.5$ at 1550 nm because of the low concentration of MR in E7 LC) and the NOA 61 refractive index equal to 1.5419 at 1550 nm. The period of

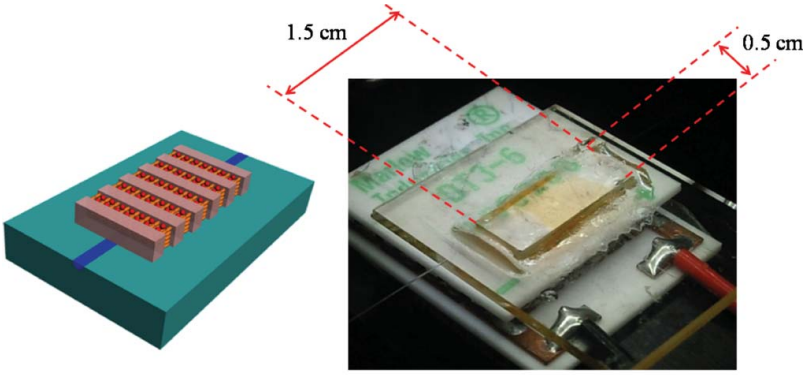


**Figure 6.** A polarization-independent all-optical Bragg filter based on photosensitive liquid crystals: schematic illustration (a) and photography (b) of the produced device under test.

the manufactured grating is estimated to be $\Lambda = 1.50$–$1.55$ $\mu$m. Considering the third diffraction order ($m = 3$), the achieved Bragg wavelength $\lambda_B$ falls in the telecom range 1520−1570 nm.

When the grating is lighted up by a pump laser source at $\lambda = 532$ nm, the MR turns in the spherical *cis* form, changing the directional order of the MR:E7 mixture. Accordingly,

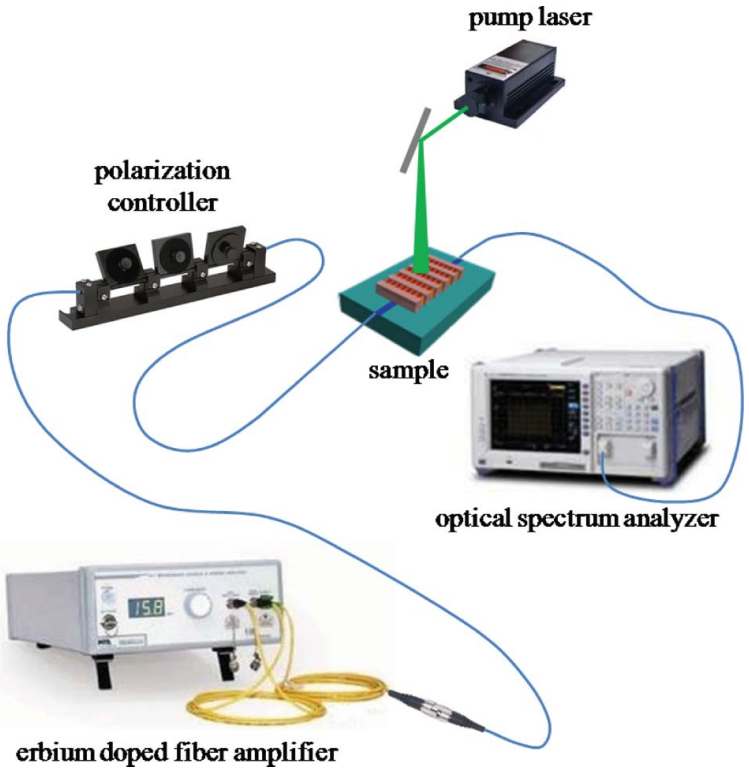


**Figure 7.** Experimental setup used to measure the all-optical Bragg filter transmittance.

there is a change in the refractive index mismatch of the grating structure, resulting in a variation of the back-reflected Bragg wavelength $\lambda_B$ depending on a variation of $n_{eff}$ in Equation (1).

The filter transmittance peak wavelength $\lambda_B$ can be controlled by switching on and off the pump signal. Therefore, the device can be used as all-optical tunable filter.

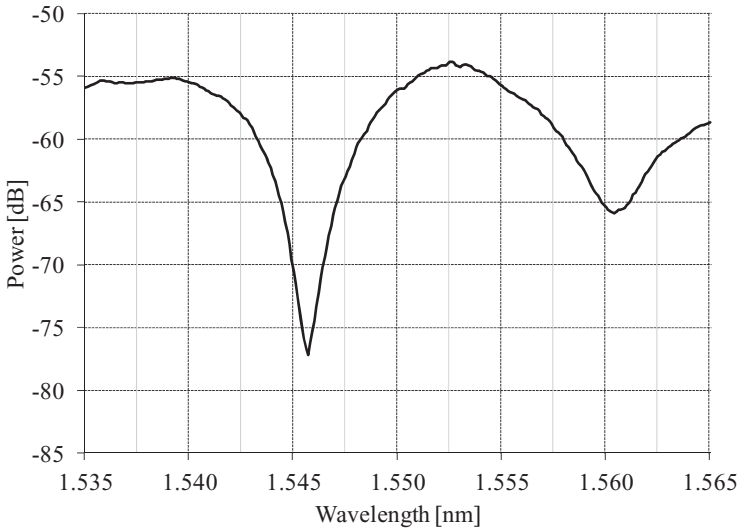


(a)

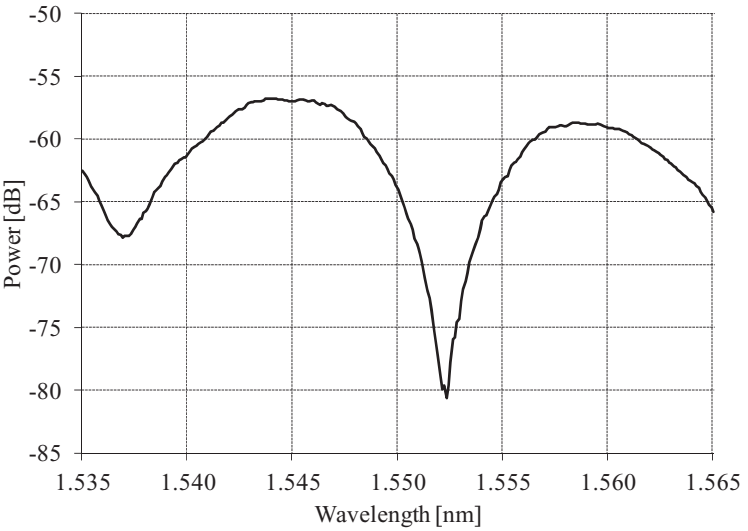


(b)

**Figure 8.** Transmitted spectra of the all-optical Bragg filter when the pump is off (a) and when the pump is on (b).

### *3.2. All-Optical Tunable Filter Characterization*

Figure 7 shows the setup used to measure the transmitted spectrum of the all-optical tunable filter. The optical signal of a broadband source between 1520 and 1580 nm, consisting of an erbium-doped fiber amplifier (EBS 4016/EDFA), is launched into the sample channel waveguide through a butt-coupled single-mode fiber. A polarization controller is inserted before the sample to select a TE polarization for the beam. The signal collected at the output of the sample is sent to an OSA. A 45 mW pump laser at $\lambda = 532$ nm, with a circular spot of about 2 mm in diameter, is used to operate the *trans-cis* transition.

Figure 8 reports the measurements of the filter transmitted spectrum. At thermal equilibrium, when the pump is off (Fig. 8(a)), the transmitted spectrum has a notch peak of $-22$ dB at $\lambda = 1545.7$ nm. Switching on the pump signal (Fig. 8(b)), the spectrum notch peak is shifted to 1552.3 nm, with the same shape but a slightly deeper notch at $-25$ dB.

An all-optical filter tuning of 6.6 nm is obtained from this prototype with a pump signal of 45 mW at 532 nm. Modeling of the Bragg wavelength shift previously reported [37] is in good agreement with measurements.

## 4. Conclusions

In a rapidly evolving communication scenario where data transmission rates are increasing toward several Terabit/second and the optical–electronic–optical bottlenecks are no longer compatible, all optical switching solutions are attracting great attention and assuming greater and greater relevance for future network solutions. In this framework, soft materials with large optical nonlinearities and low susceptibilities such as LCs are excellent candidates for low-cost low-power high-versatility efficient guided-wave solutions. In this work, we have illustrated two examples of guided-wave switches operating in the near-infrared and controlled by light. The first device is an optically controlled LCW on silicon, operating as a switch for input powers of less than 25 mW. We also discussed our experimental demonstration of an optically tunable distributed Bragg reflector exploiting the *trans-cis* transition of an azo-dye-doped LC in a periodic arrangement. Tunability over nearly 7 nm was obtained, with pump powers as small as 45 mW.

## References

[1] Ramaswami, R., Sivarajan, K. N., & Sasaki, G. H. (2010). *Optical Networks: A Practical Perspective,* 3rd ed., Morgan-Kauffmann Publishers: San Francisco, CA.
[2] O'Mahony, M. J., Politi, C., Klonidis, D., Nejabati, R., & Simeonidou, D. (2006). *J. Lightw. Technol.*, *24*, 4684.
[3] Berthold, J., Saleh, A. A. M., Blair, L., & Simmons, J. M. (2008). *J. Lightw. Technol.*, *26*, 1104.
[4] Saleh, A. A. M., Simmons, J.M. (2012). *Proc. IEEE*, *100*, 1105.
[5] Hillerkuss, D., *et al.* (2011). *Nature Photon.*, *5*, 364.
[6] Monat, C., Domachuk, P., & Eggleton, B. J. (2007). *Nature Photon.*, *1*, 106.
[7] Psaltis, D., Quake, S. R., & Yang, C. H. (2006). *Nature*, *442*, 381.
[8] Schmidt, H., & Hawkins, A. R. (2011). *Nature Photon.*, *5*, 598.
[9] Woltman, S. J., Jay, G. D., & Crawford, G. P. (2007). *Nature Mater.*, *6*, 929.
[10] Khoo, I. C. (2007). *Liquid Crystals, 2nd ed.*, Wiley: New York.
[11] Khoo, I. C. (2011). *J. Opt. Soc. Am.*, *28*, A45.
[12] Simoni, F. (1997). *Nonlinear Optical Properties of Liquid Crystals and Polymer Dispersed Liquid Crystal*, World Scientific: Singapore.
[13] Khoo, I.C., Slussarenko, S., Guenther, B.D., & Wood, W.V. (1998). *Opt. Lett.*, *23*, 253.
[14] Lucchetti, L., Di Fabrizio, M., Francescangeli, O., & Simoni, F., (2004). *Opt. Com.*, *233*, 417.
[15] d'Alessandro, A., & Asquini R. (2003). *Mol. Cryst. Liq. Cryst.*, *398*, 207.

[16] Beeckman, J., Neyts, K., & Vanbrabant, P. J. M. (2011). *Opt. Eng*., *50*, 081202.
[17] Zografopoulos, D. C., Asquini, R., Kriezis, E. E., d'Alessandro, A., & Beccherelli, R. (2012). *Lab Chip.*, *12*, 3598.
[18] Coles, H., & Morris, S. (2010). *Nature Photon*., *4*, 676.
[19] De Sio, L., Cuennet, J. G., Vasdekis, A. E., & Psaltis, D. (2010). *Appl. Phys. Lett*., *96*, 131112.
[20] Cuennet, J. G., Vasdekis, A. E., De Sio, L., & Psaltis, D. (2011). *Nature Photon*., *5*, 234.
[21] Liu, Y., Cheng, D., Lin, I. H., Abbott, N. L., & Jiang, H. (2012). *Lab Chip.*, *12*, 3746.
[22] Asquini, R., Fratalocchi, A., d'Alessandro, A., & Assanto, G. (2005). *Applied Optics*., *44*, 4136.
[23] Fratalocchi, A., Asquini R., & Assanto, G. (2005). *Opt. Express.*, *13*, 32.
[24] Asquini, R., Donisi, D., Trotta, M., d'Alessandro, A., Bellini, B., Gilardi, G. & Beccherelli, R. (2009). *Mol. Cryst. Liq. Cryst*., *500*, 23.
[25] Donisi, D., Bellini, B., Beccherelli, R., Asquini, R., Gilardi, G., Trotta, M., & d'Alessandro, A. (2010). *IEEE J. Quantum Electron*., *46*, 762.
[26] Donisi, D., Asquini, R., d'Alessandro, A., Bellini, B., Beccherelli, R., De Sio, L., & Umeton, C. (2010). *Mol. Cryst. Liq. Cryst*., *516*, 152.
[27] d'Alessandro, A., Donisi, D., De Sio, L., Beccherelli, R., Asquini, R., Caputo, R., & Umeton, C. (2008). *Opt. Express*, *16*, 9254, and (2011) Patent US 7925124 B2.
[28] Adikan, F. R. M., Gates, J. C., Dyadyusha, A., Major, H. E., Gawith, C. B. E., Sparrow, I. J. G., Emmerson, G. D., Kaczmarek, M., & Smith, P. G. R. (2007). *Opt. Lett*., *32*, 1542.
[29] Donisi, D., Asquini, R., d'Alessandro, A., & Assanto G. (2009). *Opt. Express*., *17*, 5251.
[30] Gilardi, G., Asquini, R., d'Alessandro, A., & Assanto, G. (2011). *Mol. Cryst. Liq. Cryst*., *549*, 62.
[31] Asquini, R., Gilardi, G., d'Alessandro, A., & Assanto, G. (2011). *Opt. Eng*., *50*, 071108.
[32] Gilardi, G., Asquini, R., d'Alessandro, A., & Assanto, G. (2010). *Opt. Express*., *18*, 11524.
[33] Trotta, M., Asquini, R., d'Alessandro, A., & Beccherelli, R. (2011). *Mol. Cryst. Liq. Cryst*., *549*, 100.
[34] d'Alessandro, A., Asquini, R., Trotta, M., Gilardi, G., Beccherelli, R., & Khoo I. C. (2010). *Appl. Phys. Lett*., *97*, 093302.
[35] Trotta, M., Asquini, R., d'Alessandro, A., & Beccherelli R. (2012). *Mol. Cryst. Liq. Cryst*., *558*, 204.
[36] Gilardi, G., Asquini, R., d'Alessandro, A., Beccherelli, R., De Sio L., & Umeton C. (2012). *Mol. Cryst. Liq. Cryst*., *558*, 64.
[37] Gilardi, G., De Sio, L., Beccherelli, R., Asquini, R., d'Alessandro, A., & Umeton, C. (2011). *Optics Letters.*, *36*, 4755.
[38] Assanto G., & Peccianti, M. (2003). *IEEE J. Quantum Electron*., *39*, 13.
[39] Henninot, J.F., Debailleul, M., Asquini, R., d'Alessandro, A., & Warenghem, M. (2004). *J. Opt. A: Pure Appl. Opt*., *6*, 315.
[40] Piccardi, A., Trotta, M., Kwasny, M., Alberucci, A., Asquini, R., Karpierz, M., d'Alessandro, A., & Assanto, G. (2011). *Appl. Phys. B: Lasers Optics*., *104*, 805.
[41] Peccianti M. & Assanto, G. (2012). *Phys. Rep*., *516*, 147.
[42] Peccianti, M., Conti, C., Assanto, G., De Luca, A., & Umeton, G. (2002). *Appl. Phys. Lett*., *81*, 3335.
[43] Izdebskaya, Y., Rebling, J., Desyatnikov, A., Assanto, G., & Kivshar, Y. (2012). *Opt. Express*., *20*, 24701.
[44] d'Alessandro, A., Bellini, B., Donisi, D., Beccherelli, R., & Asquini, R. (2006). *IEEE J. Quantum Electron*., *42* (*10*), 1084.
[45] d'Alessandro, A., Asquini, R., Trotta, M., & Beccherelli R. (2010). Nonlinear, Photorefractive, and Electro-Optics. In: I. C. Khoo (Ed.), *Liquid crystals XIV: Proceedings of SPIE, 7775*, SPIE: Bellingham, WA, p. 777510.
[46] Caputo, R., De Luca, A., De Sio, L., Pezzi, L., Strangi, G., Umeton, C., Veltri, A., Asquini, R., d'Alessandro, A., Donisi, D., Beccherelli, R., Sukhov A.V. & Tabiryan, N.V. (2009). *J. Opt. A: Pure Appl. Opt*., *11*, 024017.
[47] De Sio, L., Serak, S., Tabiryan, N., & Umeton, C. (2011). *J. Mater. Chem*., *21*, 6811.